DIAGONAL HORN GAUSSIAN EFFICIENCY ENHANCEMENT BY DIELECTRIC LOADING FOR SUBMILLIMETER WAVE APPLICATION AT 150 GHz

O. Xu

State Key Laboratory of Millimeter Waves
Southeast University, Nanjing, Jiangsu 210096, China

Abstract—The dielectric pyramid loaded and the dielectric cone loaded diagonal horn working at 150 GHz are investigated by using Gaussian beam mode analysis. With extremely low cross-polarized and axially symmetrical field distribution in the horn aperture, the calculated fundamental Gaussian mode coupling achieves about 98%. The far field radiation patterns of the two antennas are analyzed using fundamental Gaussian mode aperture-field distribution model whose results agree with high-accuracy CST$^{\text{TM}}$ software computations, indicating that the dielectric loaded horns radiate fine Gaussian beams. The dielectric loaded geometry may be used to modify the diagonal horns with distorted beam.

1. INTRODUCTION

Dielectric-loaded horns have been shown to provide low cross-polarization gain, low sidelobes, and symmetrical radiation due to their hybrid mode distribution in the antenna aperture [1–4]. Thus, in quasi-optical systems, a proper dielectric-loaded geometry will exhibit a high-efficiency Gaussian beam performance. Diagonal horns employ two orthogonal TE_{10} modes to generate Gaussian beams with relative high fundamental Gaussian beam mode coupling (typically 84.3%) [5, 6], and hence are attractive especially in submillimeter wave quasi-optical systems for their convenient manufacture using split block techniques. Because a relatively large amount of normal E-field exists in the metal surface, the precision assurance during fabrication process is a major factor to affect the antenna performance at submillimeter wavelengths. Defectives such as imperfect smooth surface, poor consistency of the

two halves, and relaxed fit tolerance for the split may cause the distortion of the aperture field and the decrease in the fundamental Gaussian mode coupling, resulting in high sidelobes and the asymmetry in radiation patterns. Modifications are expected to enhance the performance of these defective horns and could be achieved by dielectric loading.

Dielectric-loaded horns utilize the dominant or hybrid modes in the uniform dielectric waveguides to constitute the aperture-field distribution attenuating radially with low cross-polarization [2, 7–9]. A dielectric-loaded diagonal horn can concentrate most of the electromagnetic energy in the dielectric remaining minor fraction near the metal wall, producing a Gaussian field distribution in the dielectric cross-section [10–12]. The precision assurance problems, especially the imperfect smooth surface, will still exist in the dielectric manufacture, but the adverse effects are less serious than the metal diagonal horn case for the Gaussian field distribution. This field distribution can be used to alleviate the reduction of the fundamental Gaussian mode coupling.

In this paper, two kinds of dielectric loaded diagonal horns are investigated. They act as the radiators or receivers in a continuous wave imaging system which holds the potential applications in security check to detect the concealed objects [13–15]. The first one is the diagonal horn with a dielectric diagonal horn inside. The "dielectric diagonal horn" is presented by Tiwari et al. [16, 17], and their analysis on the near field and radiation pattern validates its low cross-polarization performance. This composite structure is called the "dielectric pyramid loaded horn" in the following content. The metal diagonal horn acts as a tapered transition between the metal waveguide and the dielectric diagonal horn and prevents the leaky radiation in a single dielectric horn. The fundamental Gaussian mode coupling of this dielectric loaded horn is analyzed numerically and the results show that a considerably high value about 98% is achieved.

The second geometry to improve the Gaussian beam of a diagonal horn is the dielectric cone loaded horn. Lier and Olver et al. have made detailed analysis on the dielectric cone loaded conical horns [1, 2]. The dielectric cone supports HE_{11} mode which contributes to low cross-polarization, low sidelobes, and a well qualified Gaussian beam for the diagonal horn. The calculation of the fundamental Gaussian mode coupling also achieves about 98%.

The far field patterns of the two dielectric loaded horns are computed by assuming that only the fundamental 00th Gaussian beam mode exists in the horn aperture. The results agree with CST^{TM} software simulations very well, suggesting that the radiated beams are

near totally responsible by the fundamental Gaussian beam mode. This confirms the high value of the fundamental Gaussian mode coupling.

2. GAUSSIAN MODE ANALYSIS

Under an axially symmetrical and well-collimated beam assumption, the electric field radiated from a quasioptical radiator can be expressed in terms of the polynomial of Gaussian-Hermite beam modes [5]:

$$\mathbf{E}(x, y, z) =$$
$$\frac{w_A}{w(z)} \exp[-jk(z-z_A)] \cdot \exp[j(\Phi(z)-\Phi_A)] \cdot \exp\left[-jk\left(x^2+y^2\right)/2R(z)\right]$$
$$\cdot \sum_{m=0}^{\infty} \sum_{n=0}^{\infty} \left\{ \sqrt{\frac{1}{2^{m+n}m!n!}} \left(\hat{y}A_{mn} + \hat{x}B_{mn}\right) \cdot \exp[j(m+n)(\Phi(z)-\Phi_A)] \right.$$
$$\left. \cdot \exp\left[-\left(\frac{x}{w(z)}\right)^2 - \left(\frac{y}{w(z)}\right)^2\right] \cdot H_m\left[\frac{\sqrt{2}x}{w(z)}\right] \cdot H_n\left[\frac{\sqrt{2}y}{w(z)}\right] \right\} \qquad (1)$$

where $H_m(x)$ is the Hermite polynomial of order m. The beam width ($w(z)$), the phase radius of curvature ($R(z)$), and the phase slippage per beam mode ($\Phi(z)$) are basic beam parameters and are given by $w(z) = w_0\sqrt{1 + (z/z_c)^2}$, $R(z) = z[1 + (z_c/z)^2]$, $\Phi(z) = \arctan(z/z_c)$, and $z_c = \pi w_0^2/\lambda$. The horn is placed along the z-axis of the Cartesian coordinate system which is shown in Fig. 1.

For the convenience of Gaussian mode model analysis, the aperture field $\mathbf{E}_A$ of a dielectric loaded diagonal horn is expected to have its phase variation be contained in a spherical phase factor [5].
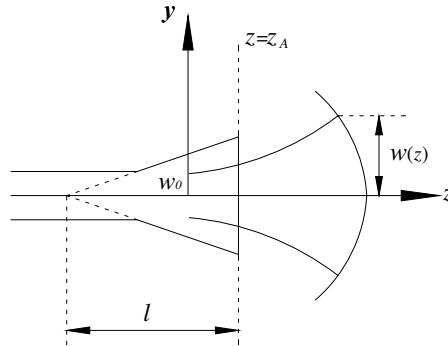
Figure 1. The coordinate system for the Gaussian beam analysis.

With this restriction, $\mathbf{E}_A$ can be written as

$$\mathbf{E_A}(x,y) = [f(x,y)\hat{y} + g(x,y)\hat{x}] \cdot \exp\left[-jk\left(x^2 + y^2\right)/2R_A\right] \quad (2)$$

The phase radius of curvature at the horn aperture plane (R_A) is set to the length of the horn (l) indicated in Fig. 1 by adjusting the value of Φ_A, leading to real-valued amplitudes of $\mathbf{E}_A$, denoted by $f(x,y)$ and $g(x,y)$. Then the undetermined coefficients A_{mn} and B_{mn} in (1) are given by [5, 18]:

$$A_{mn} = \frac{2}{\pi w_A^2} \iint\limits_{Aperture} f(x,y) \sqrt{\frac{1}{2^{m+n}m!n!}} \exp\left[-\left(\frac{x}{w(z)}\right)^2 - \left(\frac{y}{w(z)}\right)^2\right]$$

$$\cdot H_m\left[\frac{\sqrt{2}x}{w(z)}\right] \cdot H_n\left[\frac{\sqrt{2}y}{w(z)}\right] dxdy \quad (3)$$

$$B_{mn} = \frac{2}{\pi w_A^2} \iint\limits_{Aperture} g(x,y) \sqrt{\frac{1}{2^{m+n}m!n!}} \exp\left[-\left(\frac{x}{w(z)}\right)^2 - \left(\frac{y}{w(z)}\right)^2\right]$$

$$\cdot H_m\left[\frac{\sqrt{2}x}{w(z)}\right] \cdot H_n\left[\frac{\sqrt{2}y}{w(z)}\right] dxdy \quad (4)$$

The fundamental Gaussian mode coupling, representing the fractional power in the 00th Gaussian beam mode, is formulated by

$$\eta_G = \frac{P_{00}^{co}}{P_{tot}} = \frac{\pi w_A^2}{2} \frac{|A_{00}|^2}{\iint\limits_{Aperture}\left[|f(x,y)|^2 + |g(x,y)|^2\right] dxdy} \quad (5)$$

The parameter w_A/a is usually chosen so that η_G is maximized:

$$\frac{\partial \eta_G}{\partial(w_A/a)} = 0 \quad (6)$$

where a is the aperture radius of the antenna.

For a regular geometry such as a single metal horn or a single dielectric antenna, the field in the aperture of the horn can be expressed either accurately or asymptotic analytically, but the dielectric-loaded diagonal horn complicates the guided mode analysis at the aperture. Instead of mathematical manipulations towards the inhomogeneous waveguide model, we extract the discrete electric field $\mathbf{E}_A(x_i, y_i)$ in the horn aperture from CST^{TM} software results due to its accuracy and convenience in dealing with arbitrary dielectric-loaded geometries [19]. Then numerical integrals and numerical differentials can be performed

in (3)–(6) to obtain η_G. However, according to (2), the phase variation in the horn aperture must yield to a spherical phase factor, and the dielectric shape or dimension will be carefully optimized with the assistance of CST$^{\text{TM}}$ software to satisfy this restriction in the following analysis. A satisfactory spherical phase front is principally depended on the reasonable taper angle of the dielectric pyramid. When the working frequency is changed a lot, the phase variation in the aperture may be distorted, resulting in a failure Gaussian mode analysis even though the radiation performances, such as gain and the co-polarization are kept in a satisfactory level. Hence a single frequency (150 GHz) will be discussed in the following analysis, and is sufficient for a continuous wave imaging system.

3. DIELECTRIC PYRAMID LOADED DIAGONAL HORN ANALYSIS

The first dielectric-loaded diagonal horn working at 150 GHz is illustrated in Fig. 2. The aperture of the metal horn and the dielectric insertion (Teflon, $\varepsilon_r = 2.1$, Loss tangent = 0.0004) are square, with the optimized side length $2a = 10$ mm and $2d = 7.07$ mm, respectively. The longitudinal length (l) of the two horns are coincide, and $l = 22$ mm. The metal diagonal horn is fed by a WR6 waveguide with inside dimensions 1.6×0.8 mm which is matched to a rectangular dielectric waveguide by a wedge. The rectangular dielectric waveguide is inserted directly into the 45°-rotated dielectric diagonal horn presented by

(a)   (b)
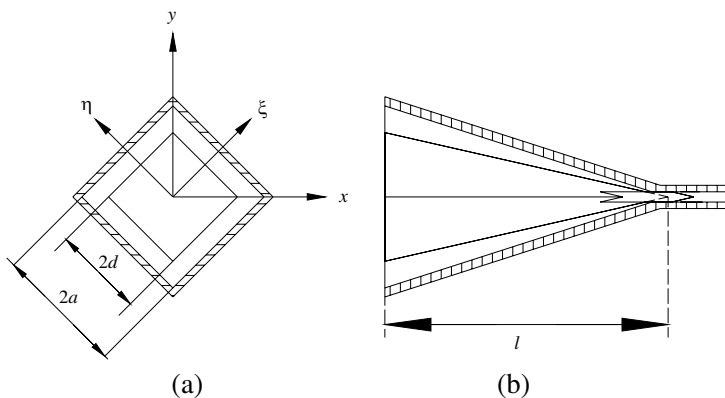
Figure 2. The geometry of the dielectric pyramid loaded diagonal horn. (a) Front view of the geometry with the coordinate frame definition. (b) Side view of the dielectric pyramid with the metal diagonal horn longitudinally cut.
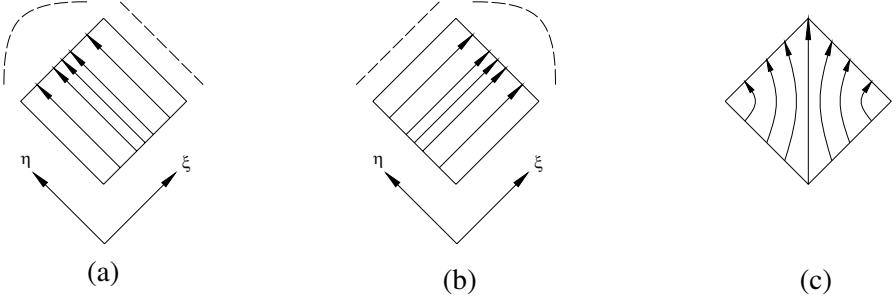
Figure 3. The electric field distribution in the aperture of a metal diagonal horn. (a) TE_{10}^{η} mode with electric field $\hat{\eta}$-directed, whose amplitude varies as cosine function with ξ and keeps constant with η. (b) TE_{10}^{ξ} mode with electric field $\hat{\xi}$-directed, whose amplitude varies as cosine function with η and keeps constant with ξ. (c) The superposition of the two modes with equal amplitudes and zero phase difference.

Tiwari et al. [16, 17].

The electric field distribution in the aperture of a single metal diagonal horn consists of two orthogonal TE_{10} modes, that is, the sum of TE_{10}^{η} and TE_{10}^{ξ} modes where the $\xi\eta$ coordinate system is defined in Fig. 2(a). A sketch of the two mode patterns is plotted in Fig. 3, where the invariableness of the electric field along $\hat{\eta}$-direction in Fig. 3(a) or along $\hat{\xi}$-direction in Fig. 3(b) results in the considerable large cross-polarized ($\hat{x}$-directed) field component. For an idealized single dielectric diagonal horn, the aperture field consists chiefly of E_{11}^{η} and E_{11}^{ξ} modes shown in Fig. 4 [20]. The cosine variation along both $\hat{\eta}$-direction and $\hat{\xi}$-direction contributes to extremely low cross-polarization level in the dielectric aperture and to considerable minimal amplitude at the four aperture edges.

With a well-designed transition and carefully optimized parameters sketched in Fig. 2, the energy in the intrinsic modes of the metal diagonal horn (TE_{10}^{η} plus TE_{10}^{ξ}) will be coupled efficiently into the intrinsic modes of dielectric horn (E_{11}^{η} plus E_{11}^{ξ}) for the quite similar distribution of the two sets of modes.

3.1. Numerical Analysis

Using CST^{TM} software, the discrete electric field $\mathbf{E}_A(x_i, y_i)$ in the horn aperture is extracted, containing $f(x_i, y_i)$, $g(x_i, y_i)$, and the phase located at every discrete point. The polarization efficiency ζ, which is calculated as the ratio of the co-polarized ($\hat{y}$-directed) powers to
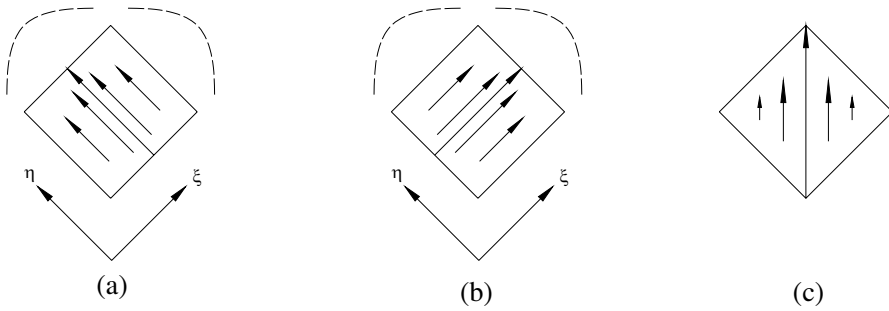
Figure 4. The electric field distribution in the aperture of an idealized dielectric diagonal horn. (a) E_{11}^{η} mode with electric field $\hat{\eta}$-directed, whose amplitude varies as cosine function with both ξ and η. (b) E_{11}^{ξ} mode with electric field $\hat{\xi}$-directed, whose amplitude varies as cosine function with both ξ and η. (c) The superposition of the two modes with equal amplitude and zero phase difference.
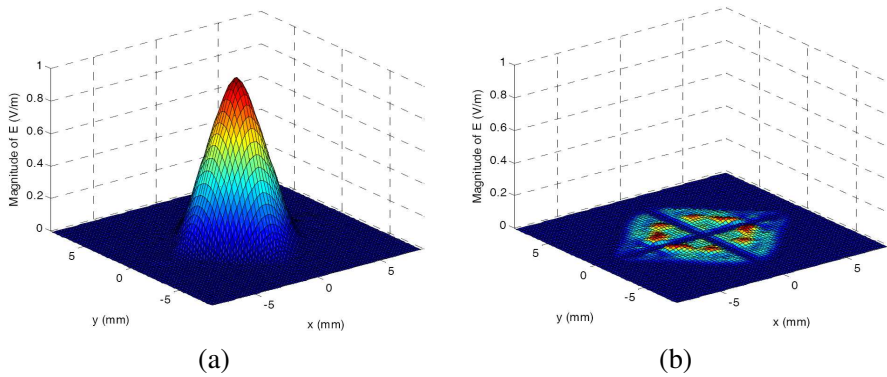
Figure 5. The magnitude of the co-polarized and cross-polarized field components at the aperture of the dielectric pyramid loaded horn. (a) Co-polarized component, with good axially symmetrical performance and fine Gaussian distribution. (b) Extremely low cross-polarized component.

total powers ($\zeta = P_{co}/P_{tot}$), is obtained by numerical integral over the aperture, and the result is 99% which is relatively high compared with the single diagonal horn case (typically 90.5% [5]). The magnitudes of co-polarized field ($|f(x_i, y_i)|$) and cross-polarized field ($|g(x_i, y_i)|$) in the aperture of the dielectric pyramid loaded horn are shown in Fig. 5 by CST$^{\text{TM}}$ simulation. Comparing with these components in a single diagonal horn case illustrated in Fig. 6 which is obtained by the
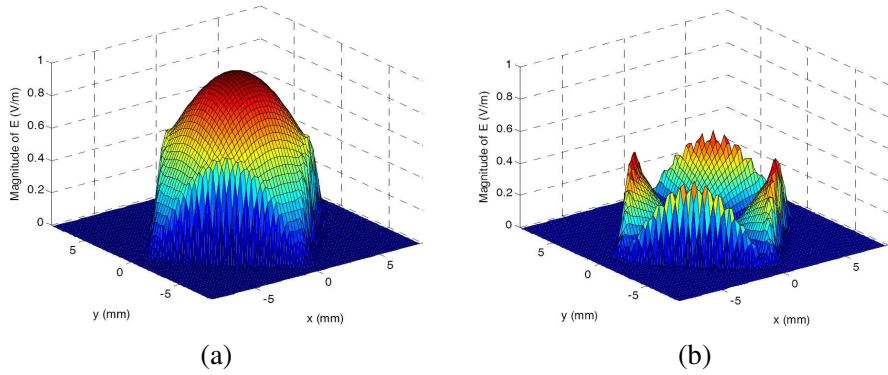
Figure 6. The magnitude of the co-polarized and cross-polarized field components at the aperture of a single diagonal horn. (a) Co-polarized component. (b) Cross-polarized component, which is quite large especially at the four edges.

analytical formula [5], the enhancement of co-polarization and axial symmetry by dielectric loading scheme is evident.
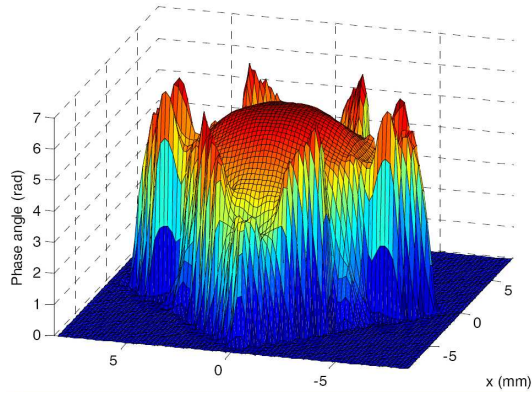
The phase angle distribution in the aperture is shown in Fig. 7. It is can be seen that most of the phase variation of the dielectric-loaded horn is contained in a spherical phase factor in the dielectric region, while abrupt peaks appear in the gap between the metal wall and the dielectric edges. The cluttery distribution in the gap is due to the different phase velocities of the two regions. However, the field in the gap is extremely low, characterized by a maximum value of -22 dB and the average value of -42 dB with respect to the amplitude at the center of the horn aperture. It is reasonable to state that the phase variation is contained in a spherical phase factor by ignoring the field in the gap. In other words, the fundamental Gaussian beam mode content η_G is principally determined by the dielectric horn aperture. Thus, the Equations (3)–(6) can be used in η_G calculation.

Substituting the aperture field $f(x_i, y_i)$ and $g(x_i, y_i)$ into (3)–(6), the fundamental Gaussian mode coupling efficiency η_G for the dielectric pyramid loaded diagonal horn is 98% for $w_A/\mathbf{a} \approx 0.5158$, or $w_A/\mathbf{d} \approx 0.7285$.

3.2. Idealized Dielectric Horn Modeling

To verify the correctness of the numerical analysis model mentioned above, it is necessary to derive an approximate analytical solution to η_G. The metal diagonal horn prevents the lateral leakage radiation from the dielectric radiator, and we notice that it has extremely

Figure 7. The phase angle distribution in the horn aperture, which is contained in a spherical surface in the dielectric region.

low field level outside of the dielectric region at the horn aperture plane, so the geometry described by Fig. 2 can be viewed as a single idealized dielectric horn with no diffractions or leakage radiations. The hybrid mode expression in the aperture of a dielectric diagonal horn is approximately to demonstrate $f(x, y)$ and $g(x, y)$ in (2)–(4).

The aperture field in the dielectric aperture is approximated by the sum of E_{11}^{η} and E_{11}^{ξ} modes with equal amplitudes and zero phase difference [16, 17, 20]:

$$f(x,y) = \left(\sqrt{2}/2\right) E_0 \cos k_\xi \left(x\sqrt{2}/2 + y\sqrt{2}/2\right) \cos k_\eta \left(y\sqrt{2}/2 - x\sqrt{2}/2\right)$$
$$+ \left(\sqrt{2}/2\right) E_0 \cos k_\xi' \left(x\sqrt{2}/2 + y\sqrt{2}/2\right) \cos k_\eta' \left(y\sqrt{2}/2 - x\sqrt{2}/2\right) \quad (7a)$$

$$g(x,y) = \left(\sqrt{2}/2\right) E_0 \cos k_\xi' \left(x\sqrt{2}/2 + y\sqrt{2}/2\right) \cos k_\eta' \left(y\sqrt{2}/2 - x\sqrt{2}/2\right)$$
$$- \left(\sqrt{2}/2\right) E_0 \cos k_\xi \left(x\sqrt{2}/2 + y\sqrt{2}/2\right) \cos k_\eta \left(y\sqrt{2}/2 - x\sqrt{2}/2\right) \quad (7b)$$

where

$$k_\xi = \frac{\pi}{2d}\left(1 + \frac{\lambda/(\sqrt{\varepsilon_r - 1})}{2\pi d}\right)^{-1}, \quad k_\eta = \frac{\pi}{2d}\left(1 + \frac{\lambda/(\sqrt{\varepsilon_r - 1})}{2\pi \varepsilon_r d}\right)^{-1} \quad \text{for } E_{11}^{\eta} \text{ mode}$$

$$k_\xi' = \frac{\pi}{2d}\left(1 + \frac{\lambda/(\sqrt{\varepsilon_r - 1})}{2\pi \varepsilon_r d}\right)^{-1}, \quad k_\eta' = \frac{\pi}{2d}\left(1 + \frac{\lambda/(\sqrt{\varepsilon_r - 1})}{2\pi d}\right)^{-1} \quad \text{for } E_{11}^{\xi} \text{ mode}$$

The coordinate system is defined in Fig. 1 and Fig. 2(a).

By substituting (7) into (3)–(4) and applying (5) and (6), the fundamental beam mode coupling, $\eta_G \approx 97\%$ is achieved for $w_A/\mathbf{a} \approx 0.5184$, or $w_A/\mathbf{d} \approx 0.7331$. This analytical solution is coincident with

the numerical result mentioned above. The numerical based Gaussian beam mode analysis has been proven to be correct by the theoretical analysis. Then the same numerical technique can be employed to investigate diverse dielectric loaded quasioptical radiators with more confidence. As an example, the Gaussian beam efficiency of a dielectric cone loaded horn is discussed in the following.
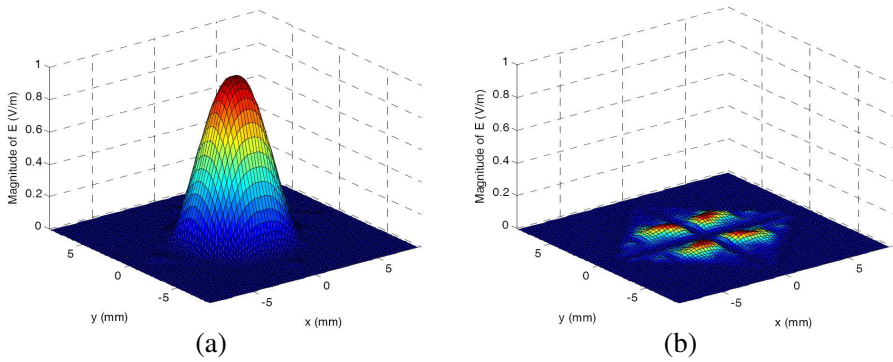
4. DIELECTRIC CONE LOADED HORN

Figure 8 shows a dielectric cone loaded diagonal horn working at 150 GHz. The same metal diagonal horn ($2a = 10$ mm and $l = 22$ mm) and the same transition wedge are employed as the dielectric pyramid loaded case. The diameter of the dielectric insertion (Teflon, $\varepsilon_r = 2.1$, Loss tangent = 0.0004) at the aperture is optimized as $2r = 8$ mm. The direct combination of the dielectric waveguide with the cone results in reflection, but will be convenient in manufacture. The HE$_{11}$ mode in the cone aperture will increase the power converted into the fundamental Gaussian beam mode and promote the symmetry of radiation patterns.


(a)   (b)
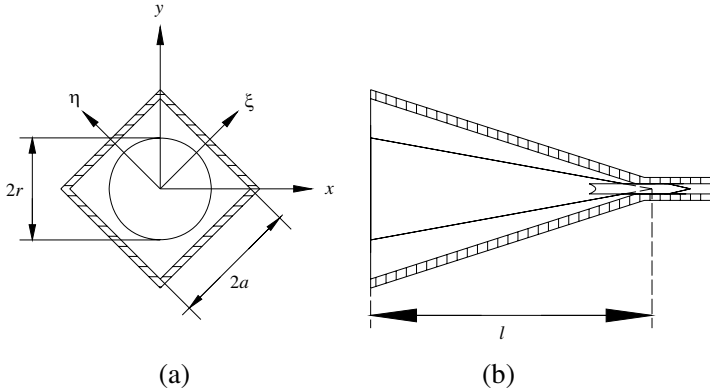
Figure 8. The geometry of the dielectric cone loaded diagonal horn. (a) Front view of the geometry with the coordinate frame definition. (b) Side view of the dielectric cone with the metal diagonal horn longitudinally cut.

The calculated value of the polarization efficiency ζ is 99%. The magnitudes of co-polarized and cross-polarized aperture field components are shown in Fig. 9, indicating a relative large co-polarization level. The phase angle distribution is plotted in Fig. 10 and is verified to be contained in a spherical phase factor in the dielectric cone aperture.

(a)   (b)

Figure 9. The magnitude of co-polarized and cross-polarized field components at the aperture of dielectric cone loaded horn. (a) Co-polarized component, with good axially symmetrical performance and perfect Gaussian distribution. (b) Extremely low cross-polarized component.
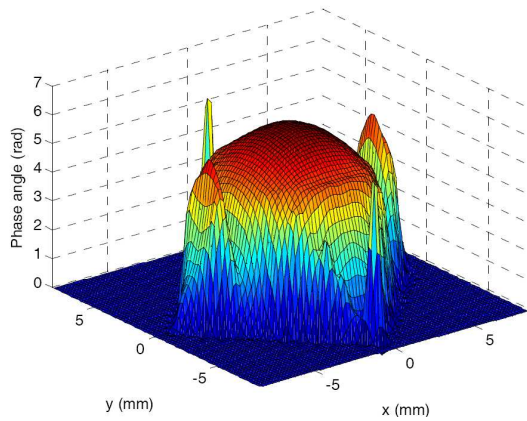
Figure 10. The phase angle distribution in the horn aperture.

Using (3)–(6) and $f(x_i, y_i)$ extracted from CST$^{\text{TM}}$ simulation, η_G is calculated to be 98% for $w_A/\mathbf{a} \approx 0.5248$, or $w_A/\mathbf{r} \approx 0.656$.

5. RADIATION PATTERN PREDICTIONS WITH FUNDAMENTAL GAUSSIAN MODE ASSUMPTION

To further verify the reasonability of the Gaussian mode analysis results, the far field radiation patterns are calculated using fundamental Gaussian mode assumption and are compared with

CST^{TM} results. The Gaussian beam mode analysis performed in part 3 and part 4 has shown that the fundamental Gaussian beam mode couplings of the two dielectric loaded horns are quite high. As a consequence, the far field pattern should be predicted correctly by assuming that only the fundamental Gaussian mode field distribution exists in the aperture. The aperture field of the horn is thus approximated by 00th Gaussian beam mode:

$$\mathbf{E}_A(x,y) = \hat{y}E_o \cdot \exp\left[-\left(\frac{x}{w(z)}\right)^2 - \left(\frac{y}{w(z)}\right)^2\right]\exp[-jk\left(x^2+y^2\right)/2l] \quad \text{(8a)}$$

$$\mathbf{H}_A(x,y) = \frac{\nabla \times \mathbf{E}_A(x,y)}{(-\mathrm{j}\omega\mu)} \quad \text{(8b)}$$

Using the equivalence principle and theS tratton-Chu equation based analysis, the far field antenna patterns can be evaluated by the following integral equation [21–24]:

$$\mathbf{E}(\mathbf{r}) = \frac{-j}{\omega\varepsilon}\int\limits_{aper}\left[k^2\mathbf{J} - (\mathbf{J}\cdot\nabla')\nabla - j\omega\varepsilon\mathbf{M}\times\nabla\right]g(\mathbf{r},\mathbf{r}')ds \quad \text{(9a)}$$

$$\mathbf{H}(\mathbf{r}) = \frac{-j}{\omega\varepsilon}\int\limits_{aper}\left[k^2\mathbf{M} - (\mathbf{M}\cdot\nabla')\nabla + j\omega\varepsilon\mathbf{J}\times\nabla\right]g(\mathbf{r},\mathbf{r}')ds \quad \text{(9b)}$$

where $\mathbf{J}$ and $\mathbf{M}$ are related to the fields on the aperture surface S by $\mathbf{J} = \hat{z}\times\mathbf{H}_A$ and $\mathbf{M} = \mathbf{E}_A\times\hat{z}$, respectively. $\boldsymbol{g(r,r')}$ is the green's function.

Figure 11 shows the normalized far field patterns of the dielectric pyramid loaded diagonal horn calculated by the fundamental Gaussian mode assumption (solid line) and CST^{TM} software (dotted line). Moreover, using Equation (9), the far field can also be predicted by the orthogonal E_{11} mode distribution in the horn aperture given by (7), which is plotted in Fig. 11 simultaneously (dashed line). The three solutions reach a good agreement. Fig. 12 shows the radiation pattern of the dielectric cone loaded horn calculated by fundamental Gaussian mode assumption (solid line) and CST^{TM} software (dotted line). The two different calculation methods exhibit good agreement. The fundamental Gaussian mode alone predicts the radiation field well.

From the radiation patterns, we can see that the dielectric cone loaded horn achieves better axially symmetrical beams than the pyramid loaded one, together with relatively low sidelobes. The field distribution in the round aperture of the cone is easier to generate a fine Gaussian beam.

CST^{TM} software performs numerical solution to integral equation according to exact antenna geometry and explains the diffraction
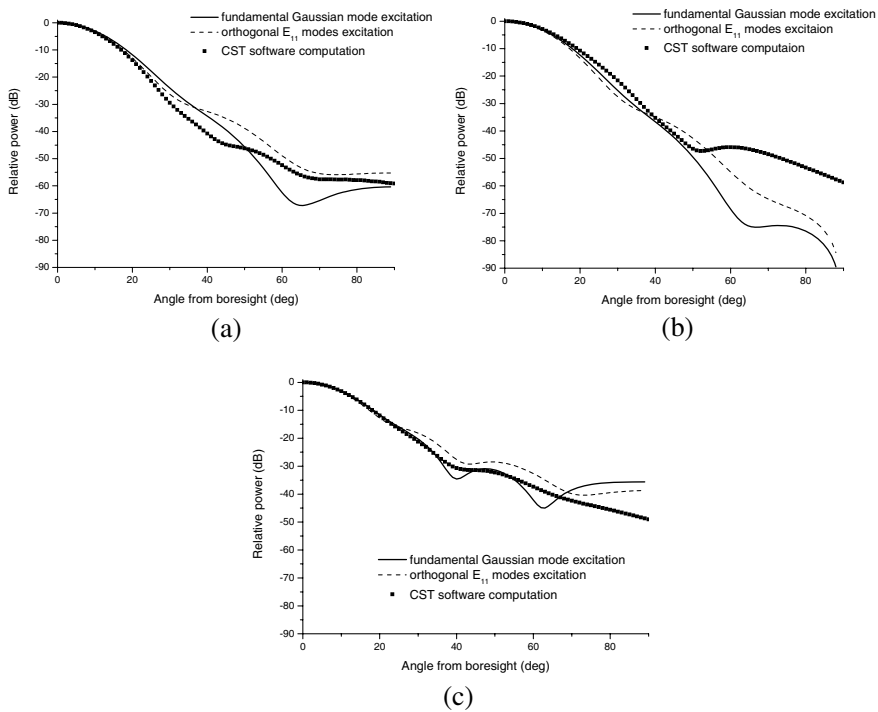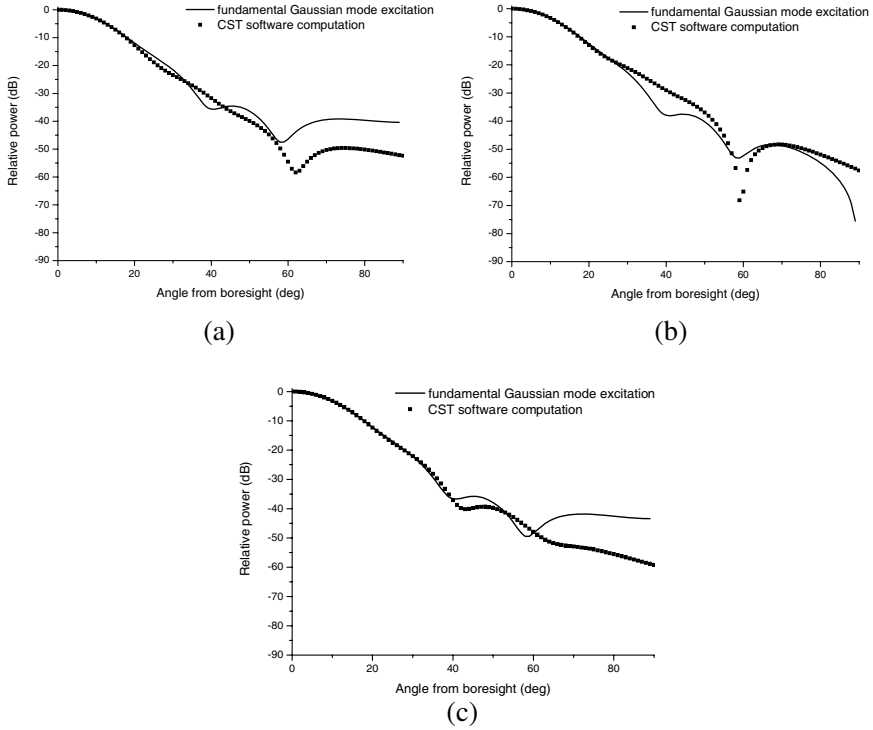
Figure 11. The far field prediction of the dielectric pyramid loaded diagonal horn at 150 GHz. (a) E-plane, (b) H-plane, and (c) D-(45°) plane.

Table 1. The calculation of the antenna gain.

Antenna type	Fundamental mode assumption	CST^{TM}
Pyramid loaded	19.5288 dB	19.35 dB
Cone loaded	19.6992 dB	19.49 dB

phenomena, so the fundamental Gaussian mode solution fails to predict the raised levels when the angle off the boresight is greater than 50° in Fig. 11(b) and is greater than 60° in Fig. 12(c).

A good agreement is also achieved for antenna gain calculation (see Table 1). CST^{TM} is a full-wave based software and its high accuracy is evident, while the fundamental Gaussian mode distribution in the aperture alone achieves relatively high accuracy, indicating the high fundamental Gaussian beam mode coupling of the two dielectric loaded diagonal horns.

(a)

(b)

(c)

Figure 12. The far field prediction of the dielectric cone loaded diagonal horn at 150 GHz. (a) *E*-plane, (b) *H*-plane, and (c) *D*-plane.

6. CROSS-POLARIZED RADIATION PATTERNS AND INPUT REFLECTIONS

Figure 13 illustrates the cross-polarized D-plane radiation patterns calculated by CST$^{\text{TM}}$ software. The solid line is the pattern of the unloaded diagonal horn, the dashed line is that of pyramid loaded horn, and the dotted line corresponds to the cone loaded one. The peak cross-polar levels of the two dielectric loaded horns are lower than −30 dB, and a reduction of 17 dB in peak level can be seen comparing with the unloaded case.

Although the Gaussian beam efficiency analysis performed in this paper is valid only at 150 GHz, the radiation properties, especially the cross-polar levels of the dielectric loaded horns, are satisfactory in the entire WR6 input waveguide band. Fig. 14 plots the peak levels of cross-polarization against frequency.
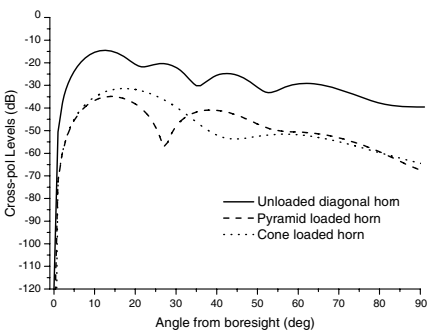
Figure 13. The cross-polarized D-plane radiation patterns.
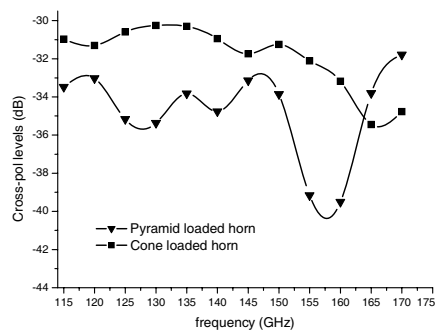
Figure 14. Peak levels of cross-polarization against frequency in WR6 waveguide band.
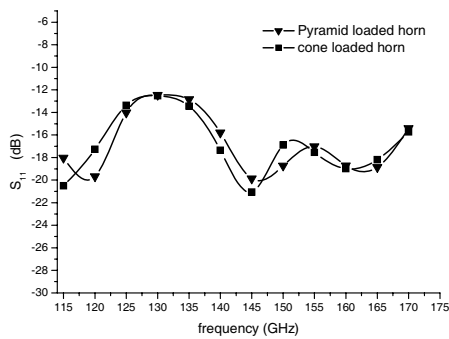
Figure 15. S_{11} values against frequency in WR6 waveguide band.

Table 2. S_{11} of the dielectric loaded horns at 150 GHz.

Antenna type	Diagonal horn	Pyramid loaded	Cone loaded
S_{11}	$-29.69\,\text{dB}$	$-18.73\,\text{dB}$	$-16.89\,\text{dB}$

However, the main drawback of the dielectric geometries is the increase of the input reflection due to the discontinuities and the dielectric loss. Table 2 lists S_{11} of the two dielectric loaded horns at 150 GHz, which are higher than that of the single diagonal horn. Fig. 15 is the S_{11} curves for the two horns as a function of the frequency, indicating a bad behavior of transmission in 125–135 GHz band where the S_{11} values approach -12 dB.

7. CONCLUSION

Gaussian mode analysis is performed to study the fundamental Gaussian mode coupling of a dielectric pyramid loaded diagonal horn and a dielectric cone loaded diagonal horn. The considerably low cross-polarized and axially symmetrical field distribution in the dielectric loaded antenna aperture contributes to quite a high fundamental Gaussian beam mode coupling. The far field analysis which assumes that only fundamental Gaussian mode in the horn aperture achieves an excellent agreement with the CST$^{\text{TM}}$ software. The dielectric pyramid loaded horn or the dielectric cone loaded horn offers a performance enhancement to the single diagonal horn. One of the benefits of using dielectric loaded horns at submillimeter wavelength will be the performance correction of antennas without extremely high precision machining.

REFERENCES

1. Lier, E., "A dielectric hybrid mode antenna feed: A simple alternative to the corrugated horn," *IEEE Transactions on Antennas and Propagation*, Vol. 34, No. 1, 21–29, 1986.

2. Olver, A. D., P. J. B. Clarricoats, and K. Raghavan, "Dielectric cone loaded horn antennas," *IEE Proceedings*, Vol. 135, No. 3, 158–162, 1988.

3. Martin, A. G., "Symmetrical low cross-polar radiation from a dielectric sphere loaded horn," *IEEE Transactions on Antennas and Propagation*, Vol. 27, No. 6, 862–863, 1979.

4. Chung, J. Y., "Ultra-wideband dielectric-loaded horn antenna with dual-linear polarization capability," *Progress In Electromagnetics Research*, Vol. 102, 397–411, 2010.

5. Johansson, J. F. and N. D. Whyborn, "The diagonal horn as a sub-millimeter wave antenna," *IEEE Transactions on Microwave Theory and Techniques*, Vol. 40, No. 5, 795–800, 1992.

6. Goldsmith, P. F., *Quasioptical Systems*, IEEE Press, New York, 1998.

7. Noor Amin, A. S., M. Mirhosseini, and M. Shahabadi, "Modal analysis of multilayer conical dielectric waveguides for azimuthal invariant modes," *Progress In Electromagnetics Research*, Vol. 105, 213–229, 2010.

8. Chang, H.-W. and Y.-H. Wu, "Analysis of perpendicular crossing dielectric waveguides with various typical index contrasts and

intersection profiles," *Progress In Electromagnetics Research*, Vol. 108, 323–341, 2010.

9. Choudhury, P. K., "TE mode propagation through tapered core liquid crystal optical fibers," *Progress In Electromagnetics Research*, Vol. 104, 449–463, 2010.

10. Chang, H.-W., Y.-H. Wu, S.-M. Lu, W.-C. Cheng, and M.-H. Sheng, "Field analysis of dielectric waveguide devices based on coupled transverse-mode integral equation — Numerical investigation," *Progress In Electromagnetics Research*, Vol. 97, 159–176, 2009.

11. Siong, C. C. and P. K. Choudhury, "Propagation characteristics of tapered core helical cald dielectric optical fibers," *Journal of Electromagnetic Waves and Applications*, Vol. 23, No. 5–6, 663–674, 2009.

12. Zhang, X. F., L. F. Shen, J.-J. Wu, and T.-J. Yang, "Backward guiding of terahertz radiation in periodic dielectric waveguides," *Journal of Electromagnetic Waves and Applications*, Vol. 24, No. 4, 557–564, 2010.

13. Liu, H. -B., H. Zhong, N. Karpowicz, Y. Chen, and X.-C. Zhang, "Terahertz spectroscopy and imaging for defense and security applications," *Proceedings of The IEEE*, Vol. 95, No. 8, 1514–1527, 2007.

14. Karpowicz, N., A. Redo, H. Zhong, et al., "Continuous-wave terahertz imaging for non-destructive testing applications," *The Joint 30th International Conference on Infrared and Millimeter Waves and 13th International Conference on Terahertz Electronics, IRMMW-THz 2005*, Vol. 1, 329–330, 2005.

15. Cooper, K. B., R. J. Dengler, N. Llombart, et al., "Concealed object contrast enhancement using radar methods in a submillimeter-wave active imager," *33rd International Conference on Infrared, Millimeter and Terahertz Waves, IRMMW-THz 2008*, 1–2, 2008.

16. Tiwari, V. N., T. Tiwari, S. P. Singh, and R. K. Jha, "Near field distribution of solid dielectric diagonal horn antennas," *International Journal of Electronics*, Vol. 82, No. 2, 167–174, 1997.

17. Tiwari, V. N. and T. Tiwari, "Study of dielectric diagonal horn antenna," *International Conference on Microwave*, 657–660, 2008.

18. Shen, T., Z. Sun, and W. Dou, "The hexagonal horn as an efficient Gaussian beam launcher," *IEEE Transactions on Antennas and Propagation*, Vol. 45, No. 7, 1173–1178, 1997.

19. Lin. X. Q., T. J. Cui, Y. Fan, and X. Liu, "Frequency

selective surface designed using electric resonant structures in terahertz frequency bands," *Journal of Electromagnetic Waves and Applications*, Vol. 23, No. 1, 21–29, 2009.

20. Marcatili, E. A. J., "Dielectric rectangular waveguide and directional coupler for integrated optics," *Bell Systems Technical Journal*, Vol. 48, No. 21, 2071–2102, 1969.

21. Elliott, R. S., *Antenna Theory and Design*, Revised edition, Wiley-Interscience, New Jersey, 2003.

22. Balanis, C. A., *Antenna Theory: Analysis and Design*, 3rd edition, Wiley-Interscience, New Jersey, 2005.

23. Zhao, X.-W., Y. Zhang, H.-W. Zhang, D. G. Donoro, S.-W. Ting, T. K. Sarkar, and C.-H. Liang, "Parallel MOM-PO method with out-of-core technique for analysis of complex arrays on electrically large platforms," *Progress In Electromagnetics Research*, Vol. 108, 1–21, 2010.

24. Thakur, J. P., W. G. Kim, and Y. H. Kim, "Large aperture low aberration aspheric dielectric lens antenna for W-band quasioptics," *Progress In Electromagnetics Research*, Vol. 103, 57–65, 2010.